Journal of Solid State Chemistry 225 (2015) 53–58

Contents lists available at ScienceDirect

Journal of Solid State Chemistry

journal homepage: www.elsevier.com/locate/jssc

Synthesis, structural and spectroscopic properties of acentric triple molybdate $Cs_2NaBi(MoO_4)_3$

A.A. Savina [a,b], V.V. Atuchin [c,d,e,*], S.F. Solodovnikov [f,g], Z.A. Solodovnikova [f], A.S. Krylov [h], E.A. Maximovskiy [i,j], M.S. Molokeev [k], A.S Oreshonkov [h,l], A.M. Pugachev [m], E.G. Khaikina [a,b]

[a] Laboratory of Oxide Systems, Baikal Institute of Nature Management, SB RAS, Ulan-Ude 670047, Russia
[b] Department of Chemistry, Buryat State University, Ulan-Ude 670000, Russia
[c] Laboratory of Optical Materials and Structures, Rzhanov Institute of Semiconductor Physics, SB RAS, Novosibirsk 630090, Russia
[d] Functional Electronics Laboratory, Tomsk State University, Tomsk 634050, Russia
[e] Laboratory of Semiconductor and Dielectric Materials, Novosibirsk State University, Novosibirsk 630090, Russia
[f] Laboratory of Crystal Chemistry, Nikolaev Institute of Inorganic Chemistry, SB RAS, Novosibirsk 630090, Russia
[g] Department of Natural Sciences, Novosibirsk State University, Novosibirsk 630090, Russia
[h] Laboratory of Molecular Spectroscopy, Kirensky Institute of Physics, SB RAS, Krasnoyarsk 660036, Russia
[i] Laboratory of Epitaxial Layers, Nikolaev Institute of Inorganic Chemistry, SB RAS, Novosibirsk 630090, Russia
[j] Laboratory of Research Methods of Composition and Structure of Functional Materials, Novosibirsk State University, Novosibirsk 630090, Russia
[k] Laboratory of Crystal Structure, Kirensky Institute of Physics, SB RAS, Krasnoyarsk 660036, Russia
[l] Department of Photonics and Laser Technology, Siberian Federal University, Krasnoyarsk 660079, Russia
[m] Laboratory of Condenced Matter Spectroscopy, Institute of Automation and Electrometry, SB RAS, Novosibirsk 90, 630090, Russia

ARTICLE INFO

Article history:
Received 3 October 2014
Received in revised form
27 November 2014
Accepted 28 November 2014
Available online 6 December 2014

Keywords:
Triple molybdate
Sodium
Cesium
Bismuth
Crystal structure
Raman spectroscopy

ABSTRACT

New ternary molybdate $Cs_2NaBi(MoO_4)_3$ is synthesized in the system Na_2MoO_4–Cs_2MoO_4–$Bi_2(MoO_4)_3$. The structure of $Cs_2NaBi(MoO_4)_3$ of a new type is determined in noncentrosymmetric space group $R3c$, $a=10.6435(2)$, $c=40.9524(7)$ Å, $V=4017.71(13)$ Å^3, $Z=12$ in anisotropic approximation for all atoms taking into account racemic twinning. The structure is completely ordered, Mo atoms are tetrahedrally coordinated, Bi(1) and Bi(2) atoms are in octahedra, and Na(1) and Na(2) atoms have a distorted trigonal prismatic coordination. The Cs(1) and Cs(2) atoms are in the framework cavities with coordination numbers 12 and 10, respectively. No phase transitions were found in $Cs_2NaBi(MoO_4)_3$ up to the melting point at 826 K. The compound shows an SHG signal, $I_{2w}/I_{2w}(SiO_2)=5$ estimated by the powder method. The vibrational properties are evaluated by Raman spectroscopy, and 26 narrow lines are measured.

1. Introduction

The bismuth-containing oxides possess rich structural diversity and promising physical properties for developed applications in catalysis, optics, nanoelectronics and nanophotonics [1–7]. The bismuth molybdates, for example $Bi_2Mo_3O_{12}$, $Bi_2Mo_2O_9$, and Bi_2MoO_6, are known for their high electrical and photoconductivity, as well as for their high photocatalytic and catalytic activity [8–16]. Besides, bismuth molybdates have been evaluated as potential gas sensors [17–19] and optical materials [20,21]. Some double molybdates of bismuth and monovalent metals, such as $MBi(MoO_4)_2$ (M=Li–Cs, Ag) and $M_5Bi(MoO_4)_4$ (M=K, Cs, Tl), show interesting physical properties and may be considered as valuable ferroelastics and ferroelectrics [22], solid-state electrolytes, [23–25] optical materials [26,27], phosphors [28] and laser-host materials [29–34]. Triple molybdate $Cs_5BiZr(MoO_4)_6$ is considered as a possible material for immobilization of cesium and other solid fission products [35].

For the recent years, the triple molybdates containing three different cations and the $(MoO_4)^{2-}$ anions have been actively searched to reveal the phase formation and basic physical properties appeared due to cation combination. Previously, the quasi-ternary systems Li_2MoO_4–M_2MoO_4–$Bi_2(MoO_4)_3$ were studied, and the $LiMBi_2(MoO_4)_4$ (M=K, Tl, Rb) phases were found [36,37]. The $LiMBi_2(MoO_4)_4$ (M=K, Tl, Rb) phases crystallize in the $BaLn_2(MoO_4)_4$ structure type (space group $C2/c$) and belong to an extended crystal family of the triple molybdates $M'M''R_2(MoO_4)_4$ [38]. Systems Li_2MoO_4–M_2MoO_4–$Bi_2(MoO_4)_3$ (M=Na, Ag) are characterized by wide homogeneity regions [39]. However, no

* Corresponding author at: Institute of Semiconductor Physics, Novosibirsk 630090, Russia. Tel.: +7 383 3308889; fax: +7 383 3332771.
E-mail address: atuchin@isp.nsc.ru (V.V. Atuchin).

http://dx.doi.org/10.1016/j.jssc.2014.11.023
0022-4596/

triple compounds or extended solid solutions were observed in the Li_2MoO_4–Cs_2MoO_4–$Bi_2(MoO_4)_3$ system [36]. On the contrary, in the Na_2MoO_4–Cs_2MoO_4–$Bi_2(MoO_4)_3$ system, the existence of two triple molybdates was revealed [40]. Unfortunately, the properties of these complex molybdates remain unknown. The present study is aimed at evaluating the structural and spectroscopic properties of triple molybdate $Cs_2NaBi(MoO_4)_3$. For this purpose, the high-quality crystal and powder samples of $Cs_2NaBi(MoO_4)_3$ were prepared by high-temperature synthesis.

2. Experimental

2.1. Preparation of materials

Commercially available MoO_3, Bi_2O_3, $Na_2MoO_4 \cdot 2H_2O$, Cs_2CO_3 (all reagent grade) were used as starting materials for the synthesis of molybdates. Simple and triple molybdates were synthesized in porcelain crucibles with thorough manual grindings of the starting reagents and reaction mixtures after every 24 h of firing. Cs_2MoO_4 was prepared by annealing a stoichiometric mixture of Cs_2CO_3 and MoO_3 in two stages (673–723 K for 25–40 h and 823 K for 60 h). $Bi_2(MoO_4)_3$ was obtained by reaction: $Bi_2O_3 + 3MoO_3 = Bi_2(MoO_4)_3$ at 723–773 K for 50 h. Anhydrous Na_2MoO_4 was obtained by calcination of the corresponding crystalline hydrate, $Na_2MoO_4 \cdot 2H_2O$, at 823–873 K. The phase purity of the prepared substances was confirmed by powder X-ray diffraction (XRD) and thermal analysis. The XRD patterns and thermal characteristics of the synthesized $Bi_2(MoO_4)_3$, Cs_2MoO_4 and Na_2MoO_4 were in accordance with the parameters tabulated in the literature.

2.2. Instrumental characterization methods

Monitoring solid-state synthesis and phase equilibration were carried out by powder XRD using a D8 ADVANCE Bruker diffractometer (VANTEC detector, Cu$K\alpha$ radiation, secondary monochromator, maximal $2\theta = 100$–140°, scan step of 0.02076°). The unit cell parameters were refined by the least-squares method using the ICDD program package. The TOPAS 4.2 [41] program was used for the Rietveld refinement.

Differential scanning calorimetric (DSC) measurements were performed on a NETZSCH STA 449F1 thermoanalyzer in the temperature range of 373–923 K with the heating/cooling rates of 10 K/min. The micromorphology of the powder sample was observed by SEM using a Hitachi—3400 N scanning electron microscope at accelerating voltage 10 kV. The chemical composition of the powder sample was estimated by energy dispersive spectrometer ≪Oxford Instruments≫ at accelerating voltage 20 kV in a wide range scan mode.

The single crystal X-ray diffraction data for structure determination were collected at room temperature on a Bruker–Nonius X8 Apex CCD area-detector diffractometer (Mo$K\alpha$ radiation, graphite monochromator, φ-scans with the scan step of 0.5°). The structure was solved and refined using the SHELX-97 package [42].

The SHG response was measured in back-scattering geometry by means of the modified Kurtz–Perry powder method [43]. The experimental setup is described in details elsewhere [44]. SHG in the sample was excited by ns pulsed radiation of an Nd:YAG laser (STA-01-7, Standa) working at $\lambda = 1064$ nm with mean power 100 mW and repetition rate 1 kHz. The SHG signal at $\lambda = 532$ nm was selected by a collimator and monochromator MDR-2, and recorded by a photomultiplier. The experimental signal was corrected for the thermal noise background recorded as a signal without the laser pump. Two-photon luminescence contributions were controlled by measurements at wavelengths above and below $\lambda = 532$ nm. The SHG signal was averaged over the 5×10^5 pump pulses. The α-SiO_2 powder with the known nonlinear optical properties was used as a reference material.

The unpolarized Raman spectra were collected in a backscattering geometry using a triple monochromator Horiba Jobin Yvon T64000 Raman spectrometer operating in a double subtractive mode, then detected by an LN-cooled charge-coupled device. The spectral resolution for the recorded Stokes side Raman spectra was set to $\sim 2\ cm^{-1}$ (this resolution was achieved using gratings with 1800 grooves/mm and 100 mm slits). The microscope system based on microscope Olympus BX41 with a 50x objective lens $f = 0.8$ mm with NA = 0.75 numerical aperture provides a focal spot diameter of about 5 μm on the sample. The single-mode argon line of 514.5 nm from a Spectra-Physics Stabilite 2017 Ar^+ laser of 5 mW on the sample was used as the excitation light source. The intensity of the laser light was adjusted to avoid the sample's heating. The wavenumber position and width of spectral lines were obtained by the least square fitting of the experimental data to the Lorentzian equation: [45]

$$I_L = \frac{A}{1 + \left((x-\omega)/(\Gamma)\right)^2}$$

where A—amplitude, ω—wavenumber, Γ—full width at half magnitude, and x—actual coordinate (wavenumber).

3. Results and discussion

3.1. Synthesis, crystal growth and characterization of $Cs_2NaBi(MoO_4)_3$

Polycrystalline $Cs_2NaBi(MoO_4)_3$ was synthesized by annealing the stoichiometric mixture of Na_2MoO_4, Cs_2MoO_4 and $Bi_2(MoO_4)_3$ at 673–773 K for 60 h. For a better sample's homogenity, the intermittent manual grindings were performed every 15 h. The final powder product of light yellow color, insoluble in water and usual organic solvents, soluble in the concentrated and dilute HCl, H_2SO_4, HNO_3. $Cs_2NaBi(MoO_4)_3$ was found to melt at 826 K. The morphology of the particles is shown in Fig. 1. The powder is formed by uniform roundish coalescent grains of ~5–25 μm in diameter. There are no faceted grains, and this indicates that recrystallization temperature of the molybdate is far above the temperature of $T = 673$–773 K used for synthesis by component interdiffusion. The EDS measurements show the presence of constituent elements only. The composition ratio Cs:Na:Bi:Mo:O = 0.08:0.04:0.03:0.13:0.71 estimated for the large area of 600 × 450 μm^2 is in reasonable relation with nominal composition Cs:

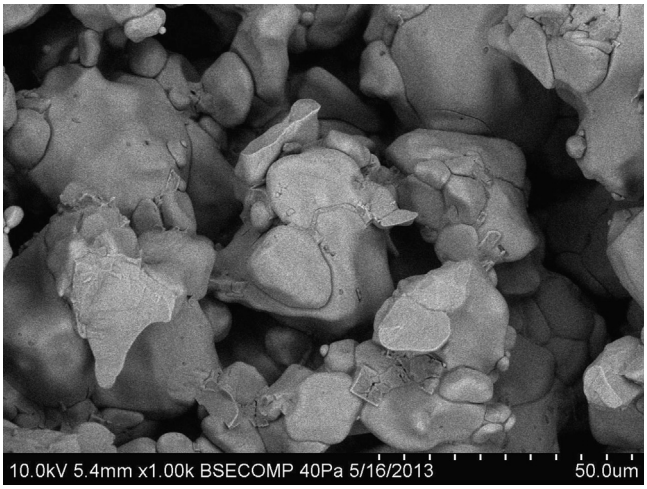

Fig. 1. SEM image of $Cs_2NaBi(MoO_4)_3$ microcrystals.

Na:Bi:Mo:O=0.11:0.05:0.05:0.16:0.63. According to the DSC measurements shown in Fig. 2, the obtained molybdate does not possess phase transitions over the temperature range of 300–826 K and melts at 826 K.

The small crystals of $Cs_2NaBi(MoO_4)_3$ applicable for structural investigation were obtained by spontaneous crystallization of the melted stoichiometric sample which was placed into the quartz crucible. Initially, the melt was held at 833 K by 0.5 h for homogenization and, after this, slow cooling was performed at the rate of 4 K/h down to 473 K. Then, the furnace was switched off and further cooled to room temperature.

3.2. Crystal structure

The structure of $Cs_2NaBi(MoO_4)_3$ was determined in noncentrosymmetric space group *R3c* in anisotropic approximation for all atoms taking into account racemic twinning. The major twin component contribution was found to be 0.529(7) at final $R=0.0200$. The acentricity of the compound was confirmed by the existence of SHG signal ($I_{2w}/I_{2w}(SiO_2)=5$) from the samples in both powder and pellet forms under laser pumping at $\lambda=1064$ nm.

Crystal data and refinement results for the $Cs_2NaBi(MoO_4)_3$ structure are summarized in Table 1. The atomic coordinates and selected interatomic distances are given in Tables 1S and 2, respectively. In the completely ordered structure, sodium, bismuth and Cs(1) atoms are at three-fold axes, whereas Cs(2), the molybdenum and oxygen atoms are located in general positions. The molybdenum atoms have a somewhat distorted tetrahedral coordination with Mo–O distances 1.702(8)–1.829(6) Å. The Bi (1) and Bi(2) atoms are in typical octahedral coordination with three shorter bond lengths and Bi–O 2.187(5)–2.617(8) Å. Analogous Bi–O distances and a similar form of BiO_6 octahedron were also found in the $Cs_5Bi(MoO_4)_4$ structure [46]. The Na(1) and Na (2) atoms have a distorted trigonal prismatic coordination with Na–O 2.383(6)–2.512(8) Å. This sodium environment is not common and encountered, for example, in the structures of $Na_{0.63}CoO_2$ [47] and $NaCo_{2.31}(MoO_4)_3$ [48] with close Na–O distances 2.350–2.513 Å and 2.31–2.40 Å, respectively. The Cs(1) and Cs(2) atoms

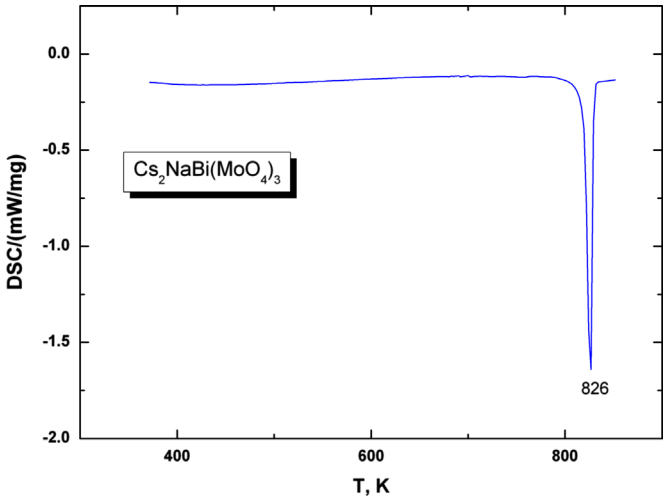

Fig. 2. The DSC curve recorded from $Cs_2NaBi(MoO_4)_3$ microcrystals.

Table 2
Selected interatomic distances (Å) in $Cs_2NaBi(MoO_4)_3$ structure.

Mo(1)-tetrahedron		**Mo(2)-tetrahedron**	
Mo(1)–O(1)	1.705(8)	Mo(2)–O(5)	1.725(7)
–O(2)	1.716(5)	–O(6)	1.738(5)
–O(3)	1.763(6)	–O(7)	1.760(6)
–O(4)	1.829(6)	–O(8)	1.814(5)
<Mo(1)–O>	1.753	<Mo(2)–O>	1.759
Cs(1)-polyhedron		**Cs(2)-polyhedron**	
Cs(1)–O(2)	3.130(5) × 3	Cs(2)–O(1)	3.070(7)
–O(5)	3.172(8) × 3	–O(5)	3.113(7)
–O(6)	3.267(4) × 3	–O(2)#1	3.114(5)
–O(1)	3.387(9) × 3	–O(2)#2	3.130(5)
<Cs(1)–O>	3.239	–O(6)#3	3.234(5)
Na(1)-polyhedron		–O(8)#4	3.347(6)
Na(1)–O(3)	2.404(9) × 3	–O(7)#4	3.360(8)
–O(7)#7	2.475(10) × 3	–O(8)#3	3.394(6)
<Na(1)–O>	2.440	–O(3)#5	3.457(8)
		–O(6)#6	3.553(6)
Na(2)-octahedron		<Cs(2)–O>	3.274
Na(2)–O(6)	2.384(6) × 3		
–O(4)	2.512(8) × 3		
<Na(2)–O>	2.448		
Bi(1)-octahedron		**Bi(2)-octahedron**	
Bi(1)–O(4)#8	2.186(5) × 3	Bi(2)–O(8)#3	2.215(5) × 3
–O(7)#1	2.617(8) × 3	–O(3)	2.565(7) × 3
<Bi(1)–O>	2.402	<Bi(2)–O>	2.390

Symmetry codes: #1 $-y+1/3, -x+2/3, z+1/6$; #2 $-x+y+1/3, y-1/3, z+1/6$; #3 $-y+2/3, -x+1/3, z-1/6$; #4 $x-1/3, x-y+1/3, z-1/6$; #5 $x+1/3, x-y+2/3, z+1/6$; #6 $-x+y+2/3, y+1/3, z-1/6$; #7 $x-2/3, y-1/3, z-1/3$; #8 $x-1/3, y-2/3, z+1/3$.

Table 1
Crystal data and structure refinement details for $Cs_2NaBi(MoO_4)_3$.

Formula	$Cs_2NaBi(MoO_4)_3$
Formula weight (g/mol)	977.61
Crystal system	Trigonal
Space group	*R3c*
Unit cell dimensions	$a=10.6435(2)$ Å
	$c=40.9524(7)$ Å
V (Å^3)/Z	4017.71(13)/12
Calculated density (g/cm^3)	4.849
Crystal size, mm	0.05 × 0.05 × 0.04
μ(Mo$K\alpha$), (mm^{-1})	21.286
θ range (deg) for data collection	2.42–28.29
Miller index ranges	$-14 \le h \le 14, -12 \le k \le 14, -42 \le l \le 54$
Reflections collected/unique	4929/1609 [R(int)=0.0383]
No. of variables	116
Goodness-of-fit on F^2 (GOF)	1.098
Final R indices [$I>2\sigma(I)$]	$R(F)=0.0200$,
	$wR(F^2)=0.0444$
R indices (all data)	$R(F)=0.0206$
	$wR(F^2)=0.0446$
Largest difference peak/hole (e Å^{-3})	0.558/−0.773

have CN 12 (icosahedron) and 10, respectively, with the joint range of distances Cs–O 3.073(8)–3.553(6) Å. Close Cs–O bond lengths 3.033–3.537 Å are observed in the $Cs_5BiZr(MoO_4)_6$ structure [35] with analogous cesium coordination numbers.

In the structure, BiO_6 octahedra share common corners with MoO_4 tetrahedra to form a very open 3D framework $[Bi(MoO_4)_3]_{3\infty}$ with the cesium and sodium ions in the framework cavities. In addition, the $Bi(2)O_6$ and $Bi(1)O_6$ octahedra are linked by common faces with $Na(1)O_6$ and $Na(2)O_6$ prisms into discrete linear four-membered polyhedral groups looking like fragments of a polyhedral column of alternating CoO_6 octahedra and CoO_6 trigonal prisms in the crystal structure of $Ca_3Co_2O_6$ [49]. A general view of $Cs_2NaBi(MoO_4)_3$ structure is given in Fig. 3.

The new structure type of $Cs_2NaBi(MoO_4)_3$ extends the series of rhombohedral framework structures of complex molybdates with $a\sim 10$ Å and long c-periods, such as $Cs_5BiZr(MoO_4)_6$ [35] of the $K_5(Mg_{0.5}Zr_{1.5})(MoO_4)_6$ [50] type ($c\approx 37$–38 Å) and $Nd_2Zr_3(MoO_4)_9$ [51] ($c\approx 58$ Å). These structures are different in compositions and symmetry; though, in all cases, the mixed frameworks $[M(MoO_4)_3]_{3\infty}$ involve discrete MO_6 octahedra and MoO_4 tetrahedra. A new characteristic detail of the $Cs_2NaBi(MoO_4)_3$ structure type is a linear group of two BiO_6 and two NaO_6 octahedra sharing common faces.

The XRD pattern recorded from the powder sample is shown in Fig. 4. All peaks, except for two very weak reflections, are successfully attributed to $Cs_2NaBi(MoO_4)_3$, and this verifies good phase purity of the powder prepared by solid state synthesis. The structural parameters obtained by Rietveld refinement were in excellent agreement with those determined by single crystal analysis.

3.3. Raman spectroscopy

The Raman spectrum recorded from the $Cs_2NaBi(MoO_4)_3$ powder is shown in Fig. 5. Additionally, the spectrum decompositions made for the local spectral ranges are shown in Figs. 1S and 2S, and the fitted parameters are presented in Table 2S. The Raman spectrum is rich in lines because of a large number of atoms. The vibrational representation of the $R3c$ structure of $Cs_2NaBi(MoO_4)_3$ at the center of the Brillouin zone has the form:

$$\Gamma_{vibr} = 38A_1 + 38A_2 + 76E$$

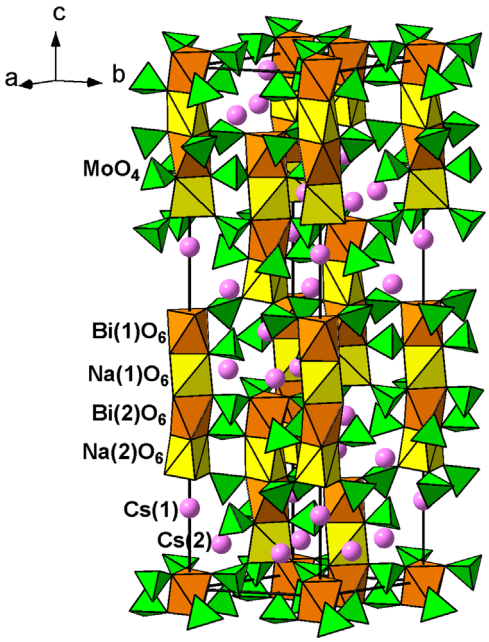

Fig. 3. A general view of the $Cs_2NaBi(MoO_4)_3$ crystal structure.

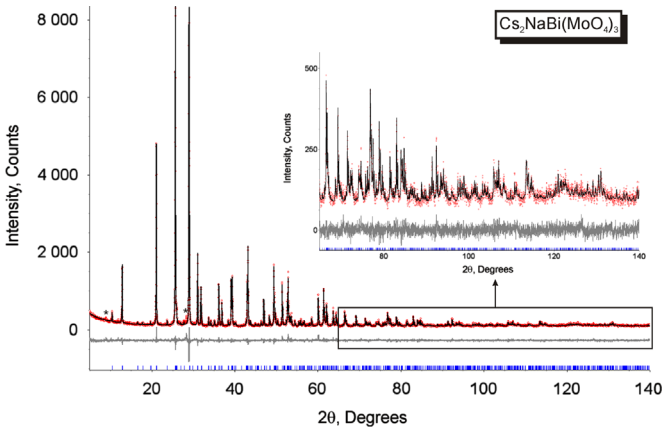

Fig. 4. The X-ray diffraction pattern recorded from the powder sample of $Cs_2NaBi(MoO_4)_3$. The impurity phase peaks are marked with asterisks.

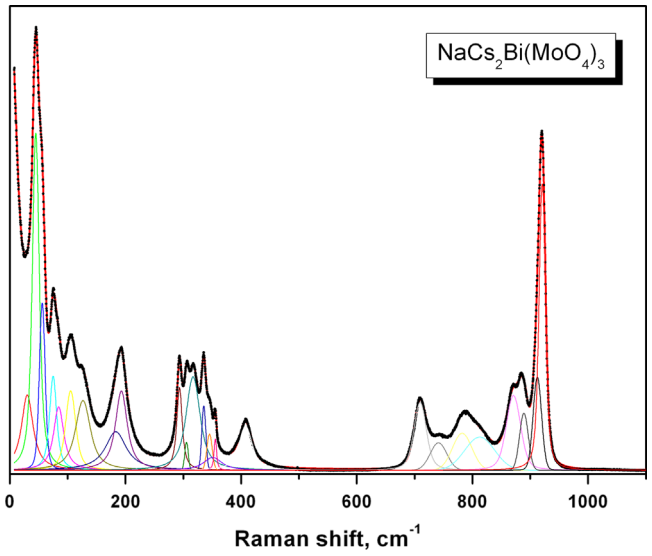

Fig. 5. The Raman spectrum obtained from $Cs_2NaBi(MoO_4)_3$ powder.

Acoustic and optic modes:

$$\Gamma_{acoustic} = A_1 + E$$

$$\Gamma_{optic} = 37A_1 + 38A_2 + 75E$$

Infrared and Raman active modes:

$$\Gamma_{Raman} = 37A_1 + 75E$$

$$\Gamma_{Infrared} = 37A_1 + 75E$$

The full spectrum could be subdivided into four parts corresponding to the vibrations of structural elements: I– $< 250\ cm^{-1}$, the region of translational, rotational and mixed vibrations of structural units; II–250–375 cm^{-1}, distorted bending modes of MoO_4 originated from undistorted modes ν_2 and ν_4; III–375–450 cm^{-1}, the region of Na–O vibrations in distorted trigonal-prismatic groups; IV–700–920 cm^{-1}, ν_1 and ν_3 MoO_4 vibrations.

To calculate the $Cs_2NaBi(MoO_4)_3$ vibrational spectrum, the program package LADY was used [52]. The calculated values of atomic vibrations were obtained using a simplified version of the Born–Karman model [53]. Previously, the optimized version of the model was tested for several compounds [54–56]. However, because of a large number of vibrational modes, a detailed interpretation of the $Cs_2NaBi(MoO_4)_3$ spectrum was quite a hard task.

[50] R.F. Klevtsova, Zh.G. Bazarova, L.A. Glinskaya, V.I. Alekseev, S.I. Arkhincheeva, B.G. Bazarov, P.V. Klevtsov, K.N. Fedorov, J. Struct. Chem. 35 (3) (1994) 286–290.
[51] R.F. Klevtsova, S.F. Solodovnikov, Yu.L. Tushinova, B.G. Bazarov, L.A. Glinskaya, Zh.G. Bazarova, J. Struct. Chem. 41 (2) (2000) 280–284.
[52] M.B. Smirnov, V.Yu. Kazimirov, LADY: Software for Lattice Dynamics Simulations. (JINR communications), E 14-2001-159, 2001.
[53] M. Smirnov, R. Baddour-Hadjean, J. Chem. Phys. 121 (2004) 2348–2355.
[54] A.S. Krylov, A.N. Vtyurin, A.S. Oreshonkov, V.N. Voronov, S.N. Krylova, J. Raman Spectrosc. 44 (5) (2013) 763–769.
[55] Y.V. Gerasimova, A.S. Oreshonkov, A.N. Vtyurin, A.A. Ivanenko, L.I. Isaenko, A.A. Ershov, E.I. Pogoreltsev, Phys. Solid State 55 (11) (2013) 2331–2334.
[56] Zhiguo Xia, M.S. Molokeev, A.S. Oreshonkov, V.V. Atuchin, Ru-Shi Liu, Cheng Dong, Phys. Chem. Chem. Phys. 16 (2014) 5952–5957.
[57] F.D. Hardcastle, I.E. Wachs, J. Phys. Chem. 95 (1991) 10763–10772.
[58] B.A. Kolesov, L.P. Kozeeva, J. Struct. Chem. 34 (4) (1993) 534–539.
[59] J. Hanuza, M. Mączka, J.H. van der Maas, J. Mol. Spectrosc 348 (1995) 349–352.
[60] H. Fuks, S.M. Kaczmarek, G. Leniec, L. Macalik, B. Macalik, J. Hanuza, Opt. Mater. 32 (2010) 1560–1567.
[61] V.V. Atuchin, O.D. Chimitova, T.A. Gavrilova, M.S. Molokeev, N.V. Sung-Jin Kim, B.G. Surovtsev, J. Cryst. Growth 318 (2011) 683–686.
[62] V.V. Atuchin, V.G. Grossman, S.V. Adichtchev, N.V. Surovtsev, T.A. Gavrilova, B.G. Bazarov, Opt. Mater. 34 (5) (2012) 812–816.
[63] V.V. Atuchin, A.S. Aleksandrovsky, O.D. Chimitova, A.S. Krylov, M.S. Molokeev, B.G. Bazarov, J.G. Bazarova, Zhiguo Xia, Opt. Mater. 36 (10) (2014) 1631–1636.
[64] S. Sheik Saleem, T.K.K. Srinivasan, Spectrochim. Acta, A 41 (12) (1985) 1419–1425.
[65] K. Nakamoto, Infrared and Raman Spectra of Inorganic and Coordination Compounds, sixth ed., Wiley, New York, NY, 2009.